Research Article

Yushi Liu, Minjie Jia, Chengzhe Song, Shuang Lu*, Hui Wang, Guanhua Zhang*, and Yingzi Yang

Enhancing ultra-early strength of sulphoaluminate cement-based materials by incorporating graphene oxide

https://doi.org/10.1515/ntrev-2020-0002
Received Dec 10, 2019; accepted Dec 18, 2019

Abstract: In order to meet the increasing engineering requirements, the ultra-early strength of sulphoaluminate cement (SAC)-based materials need to be improved to achieve road repair, engineering rescue and other objectives. Graphene oxide (GO) of 0.04 wt% was incorporated into SAC mortar to prepare GO enhanced SAC mortar (GO-SAC). It was found that the compressive strength of GO-SAC was increased by 46.9% at the age of 6 hours, and the flexural strength of GO-SAC was increased by 121.4% at the age of 100 minutes, compared with the control SAC mortar. The mechanism analysis based on the characterization results derived from XRD, BET, in situ ATR-FTIR, hydration heat measurement, TG–DSC and SEM showed that, the addition of minute quantities of GO led to the formation and growth of ribbon-like AFt, which further resulted in the improvement of the ultra-early strength of GO-SAC. This work indicates that GO has great potential for practical application in the preparation of high-performance SAC-based materials with ultra-early strength.

Keywords: sulphoaluminate cement; ultra-early strength; graphene oxide

1 Introduction

There are enormous applications of cement-based materials in the infrastructure construction [1–3], and new types of cements have attracted more and more attention because of different application performances [4, 5]. Sulphoaluminate cement (SAC) is one of the important cementitious materials [6–8], which is widely used in engineering rescue due to its early high strength characteristics, especially for occasions where engineering repairs require early strength [9–11]. In general, in order to meet the engineering application needs, SAC's early strength of 12 -24 hours needs to be focused. However, with the improvement of engineering requirements, there is a higher requirement for early strength performance [12]. Especially ultra-early strength, that is, a fast achievement of target strength within 6 hours should be widely concerned in road repair projects [13–15]. Therefore, the method of further improving the ultra-early strength of SAC needs to be solved.

One of the ways to improve the early strength of cement is to use early strength agents. Wang *et al.* [16] added 0.5% Na_2SO_4 to SAC, increasing the compressive strength at 1 day by 18.2%; S. Aggoun [17] showed that the incorporation of 0.05 wt% triethanolamine increased the compressive strength at 3 days by 50%. However, early strength agents are mainly used to increase the strength of 1-3 days, and the proportion of strength promotion is limited. Early strength agents cannot achieve ultra-early strength and have some disadvantages [18]. In particular, early strength agents containing chloride ions tend to cause steel bars in concrete to corrode more easily [19–21]. Another common method is to strengthen the early curing conditions of

***Corresponding Author: Shuang Lu:** School of Civil Engineering, Harbin Institute of Technology, Harbin 150090, China; Key Lab of Structures Dynamic Behavior and Control of the Ministry of Education, Harbin Institute of Technology, Harbin 150090, China; Key Lab of Smart Prevention and Mitigation of Civil Engineering Disasters of the Ministry of Industry and Information Technology, Harbin Institute of Technology, Harbin 150090, China; Email: lus@hit.edu.cn
***Corresponding Author: Guanhua Zhang:** Liaoning provincial transportation Planning and Design Institute Co., Ltd, Shenyang 110111, China; Email: lnzgh123@163.com
Yushi Liu, Yingzi Yang: School of Civil Engineering, Harbin Institute of Technology, Harbin 150090, China; Key Lab of Structures Dynamic Behavior and Control of the Ministry of Education, Harbin Institute of Technology, Harbin 150090, China; Key Lab of Smart Prevention and Mitigation of Civil Engineering Disasters of the Ministry of Industry and Information Technology, Harbin Institute of Technology, Harbin 150090, China
Minjie Jia: School of Civil Engineering, Harbin Institute of Technology, Harbin 150090, China
Chengzhe Song: Liaoning provincial transportation Planning and Design Institute Co., Ltd, Shenyang 110111, China
Hui Wang: Faculty of Architectural, Civil Engineering and Environment, Ningbo University, Ningbo 315000, China

Table 1: Chemical composition of SAC

Composition	CaO	Al_2O_3	SO_3	SiO_2	Fe_2O_3	TiO_2
Mass fraction (%)	45.99	21.24	13.53	8.38	2.00	0.97

concrete, with steam curing to increase strength instead of standard curing [22]. This method is obviously inefficient and uneconomical, and it can only be used for precast cement-based structural materials, also difficult to apply to engineering construction.

In recent years, considerable progress has been made in the field of "nano-concrete" [23, 24], involving the incorporation of different types of active or inactive fillers having nanoscale dimensions. Studies have shown that nanomaterials such as nano-calcium carbonate [25] and nanosilica [26] can be added to cement to increase strength as an excellent nucleating agent. At present, there are some reports on the use of nanomaterials to improve the early strength of cement-based materials, but most of them are improving the strength of 1 day and 3 days, such as Zhang and Han [27] reported that the flexural strength of reactive powder concrete (RPC) at 3 days was increased by 31.09% with 1 wt% nano-BN added; Sudipta Naskaradded [24] 1 wt% nano-TiO_2 to geopolymer concrete and the compressive strength was increased by 10% at 7 days; Qin [25] used 0.084wt% nano-calcium carbonate to improve the compressive strength of portland cement by 2.8–5.8% at 3 days; M.M.Mokhtar [28] reported that the compressive strength of ordinary portland cement was increased by 37.5% at 2 days with the addition of 0.02 wt% graphene oxide nanoplatelets. However, the effects of nanomaterials on the strength of cement within 1 day or several hours are still less clear-cut.

Graphene oxide (GO) consists of a single layer of mixed SP^2 and SP^3 hybridized carbon atoms, a single layer having a thickness of about 0.7-1 nm and a lateral dimension ranging from a few hundred nanometers to tens or hundreds of microns [29–31]. GO is functionalized with various oxygen-derived groups such as carbonyl, hydroxyl and carboxyl groups [29, 30, 32]. These oxygen groups are hydrophilic, which allows GO to form a stable colloid in water. As a derivative of graphene, GO has a high mechanical properties [33, 34] and a high specific surface area [35]. These characteristics of GO are not available in the other nanomaterials including nano-BN, nano-TiO_2, nano-$CaCO_3$ and nano-SiO_2, etc. [24, 27, 36]. Due to the unique characteristics, GO can be considered to be used as a nucleating sowing additive in cement slurries to improve its mechanical properties [28, 37–40], and the emergence of GO has presented a new opportunity to improve the earlier age strength of SAC and to achieve the ultra-early strength. Gong *et al.* stated that the compressive and tensile strength was increased by more than 40% with addition of 0.03 wt% GO into cement paste [41], and Zhu *et al.* mentioned that the compressive and tensile strength was increased by 15-33% and 41-59% by incorporation of 0.05 wt% GO in cement mortar, respectively [42]. Based on the works by Gong *et al.* and Zhu *et al.*, 0.04 wt% of GO was determined to be added to SAC for the improvement of ultra-early strength of SAC.

In this work, 0.04% weight percent GO was added to SAC to improve the ultra-early strength of SAC. We pay attention to the mechanical properties of GO enhanced SAC, including compressive and flexural strength at the ages of 100 minutes, 6 hours and 24 hours. Moreover, the influences of minute quantities of GO on microstructure, pore structure, hydration products and hydration heat of the SAC-based composite were discussed in detail. Further, the mechanism on the improved ultra-early strength of GO enhanced SAC was revealed based on the perspective of microstructure evolution.

2 Materials and methods

2.1 Raw materials

The sulphoaluminate cement produced by Dalian Cement Group with strength grade of 42.5 has a specific gravity of 2.981 and a specific surface area of 410 m^2/ kg. The chemical composition is shown in Table 1. The standard sand was purchased from Sinoma Co. Ltd (China, Xiamen). Graphite powder was purchased from Jinrilai Electronic Materials Factory (Qingdao, China). All reagents were used as received.

2.2 Preparation of graphene oxide (GO) nanosheets

1 g of graphite and 0.5 g of $NaNO_3$ were added to the flask, and then 50 ml of H_2SO_4 (98%) was added under constant stirring at 5°C for 1 hours, and then 3 g of $KMnO_4$ (1 g per 15 min) was gradually added. The temperature of the solution must be below 20°C to avoid overheating and explosion.

The solution was diluted by slowly adding 100 ml of warm distilled water, and then the solution was treated with 3 ml of a 30% H_2O_2 solution and 100 ml of distilled water to ensure complete reaction of $KMnO_4$. Thereafter, the mixture is washed with HCl and water, respectively, and finally filtered and dried to obtain a final product (GO nanosheets).

2.3 Preparation of GO enhanced SAC samples (GO-SAC)

The GO solution was diluted with deionized water in a weight percentage of 0.04% by weight of the cement and sonicated for 30 minutes. According to the Chinese standard GB/T17671-1999, a SAC mortar sample was prepared for use as a control, in which water/binder (w/b) ratio and sand/binder (s/b) ratio used were 0.50 and 3.0, respectively. According to the mix proportion of GO-SAC given in Table 2, GO-SAC was produced. A fresh mortar mixture was prepared by the same procedure using a HOBART mortar mixer and then poured into a plastic mold. The sample in the mold was covered with a plastic wrap and cured at 20 ± 2 °C for 30 min, and then demolded. The demolded samples were then cured in a standard curing chamber (20 ± 2°C, RH 95%) to 100 minutes, 6 hours, 24 hours for mechanical testing.

The fluidity of SAC and GO-SAC mortar was measured using a truncated cone with an upper diameter of 36 mm, bottom diameter of 60 mm and a height of 60 mm in accordance with Chinese standard GB/T8077-2000. The fluidity of the control SAC mortar sample (SAC) and GO-SAC mortar sample were determined to be 18.1 cm and 17.5 cm, respectively. Therefore, adding GO has little effect on the mortar fluidity due to the small amount of GO despite its high specific surface area and hydrophily.

Table 2: Mix proportion of GO-SAC

SAC/g	Water/g	GO/g	Sand/g
450	225	0.09	1350

2.4 Mechanical properties

For evaluating the mechanical properties, a set of mixtures were cast into 40 mm×40 mm×160 mm plastic molds to measure 100 minutes, 6 hours and 24 hours compressive strength and flexural strength of SAC and GO-SAC according to ISO 679:1989 and B/T 17671-1999. Before testing, the samples were cured in a curing chamber (20 ± 2°C, RH 95%). Three points bending test was carried out at a loading rate of 50 ± 10 N/s. Besides, the compressive strength test was carried out at a loading rate of 2400 ± 200 N/s.

2.5 Characterization and measurement

Atomic force microscopy images of graphene oxide (GO) were obtained using a Dimension Icon atomic force microscope (AFM, Bruker Co., Germany). Raman spectra were recorded with a Renishaw in Via Raman microscope (Renishaw Corporation, Britain) by an argon-ion laser at an excitation wavelength of 532 nm. The microstructures of SAC and GO-SAC were examined with an environmental scanning electron microscope (SEM, FEI Co., Quanta 200) with an energy dispersive X-ray spectroscope (EDS) attached. The pore structure of the sample was measured by a BET absorption method. The cement slurry samples were vacuum degassed at 80°C for 24 hours prior to measurement. Nitrogen (N_2) was used as the adsorbate. Measurements were made by surface area and pore analyzer (ASAP 2020 V3.00 H, Micromericits Company). The pore volume and pore size were calculated based on the amount of adsorbed N_2. XRD patterns were performed by an X'Pert PRO diffractometer with Cu-Kα radiation (λ = 0.15419 nm) over a 2θ range from 5° to 45°. DSC–TG analysis was performed to further examine the hydration products. The thermal properties of SAC and GO-SAC powders of about 10 mg were simultaneously measured using a DSC instrument (STA 449 F3, Netzsch) under a controlled system (20°C to 750°C, heating rate 10°C/min; nitrogen atmosphere). The hydration heat flow curve was determined by using a conduction calorimeter (TAM Air) operating at 20°C. The test cement slurry was injected into a glass ampoule by a syringe, and the same weight of air-water was injected into another glass ampoule as a reference, and the hydration heat flow of the tested cement slurry was continuously recorded over time. In situ ATR measurements were performed on ATR spectrometer (is 10, Thermo Fisher) to observe changes in hydration products.

3 Results and discussion

3.1 Mechanical properties of the GO-SAC samples at early ages

Figure 1 shows the mechanical properties of the control SAC and GO-SAC samples at 100 minutes, 6 hours and

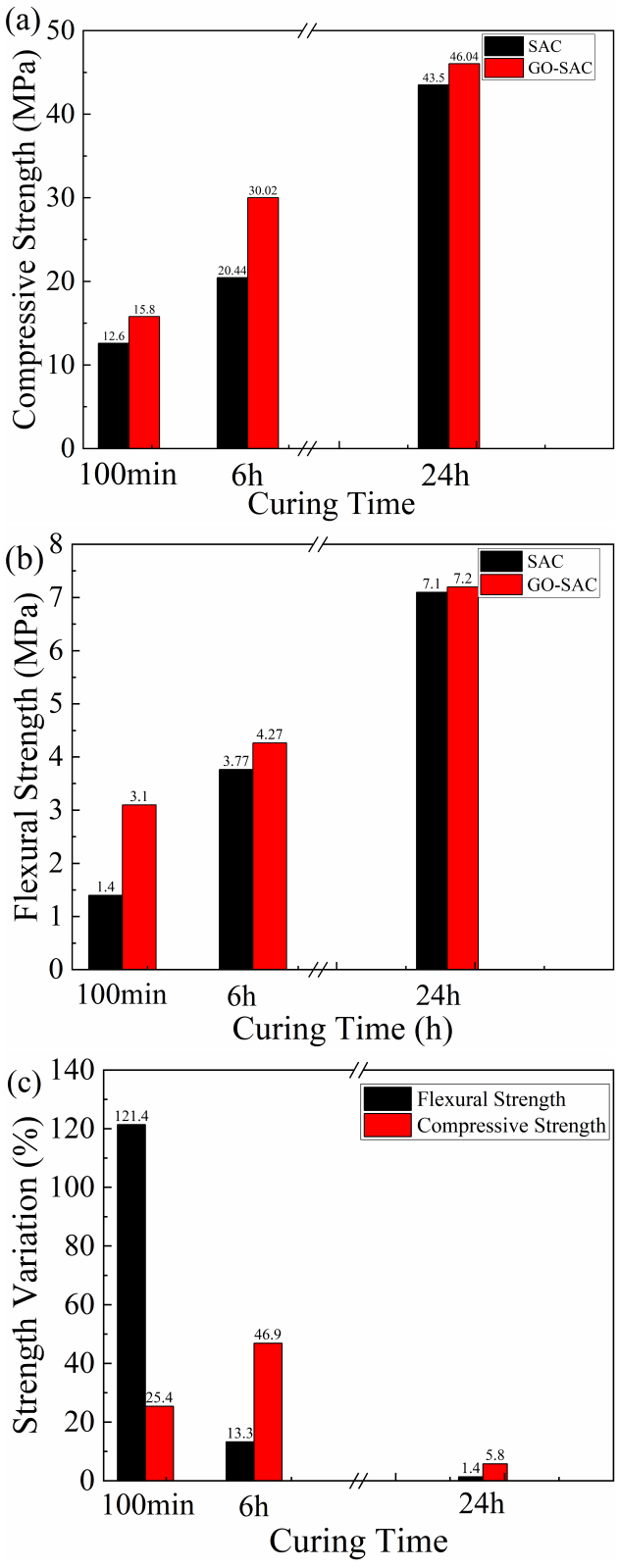

Figure 1: Mechanical properties of GO-SAC and SAC at 100 min, 6 h and 24 h. (a) the compressive strength; (b) flexural strength of samples; (c) the strength variation of samples at different ages

24 hours. From Figure 1, the compressive and flexural strength of the control SAC and GO-SAC samples increase with increasing curing time from 100 minutes to 24 hours. And the results indicate that the compressive and flexural strength are increased by the addition of 0.04 wt% GO at early ages including 100 minutes, 6 hours and 24 hours. From Figure 1a, the compressive strength of the control SAC samples at 100 minutes, 6 hours and 24 hours are 12.6 MPa, 20.44 MPa and 43.5 MPa, respectively. While as for the GO-SAC samples, the compressive strength at 100 minutes, 6 hours, and 24 hours are 15.8 MPa, 30.02 MPa and 46.04 MPa, respectively. As shown in Figure 1c, the compressive strength of GO-SAC are 25.4%, 46.9% and 5.8% higher than that of SAC at 100 minutes, 6 hours, and 24 hours, respectively. Moreover, from Figure 1b, the flexural strength of control SAC at 100 minutes, 6 hours and 24 hours are 1.4 MPa, 3.77 MPa and 7.1 MPa, respectively, and it is determined to be 3.1 MPa, 4.27 MPa and 7.2 MPa for the GO-SAC samples at 100 minutes, 6 hours and 24 hours. In Figure 2c, the flexural strength of GO-SAC are increased by 121.4%, 13.3% and 1.4% compared with control SAC at 100 minutes, 6 hours, and 24 hours. Although the incorporation of 0.04 wt% GO can improve the early strength of SAC, especially the compressive strength at 6 hours is increased by 46.9% and the flexural strength at 100 minutes is increased by 121.4%. However, with the growth of age, the increase of compressive and flexural strength becomes more and more gentle with increasing curing time. Since the compressive strength is significant dependent on microstructure compactness, and the flexural strength is more dependent on the morphology of the hydration products. It can be suggested that GO promotes the formation of hydration products with new morphology which can enhance the flexural strength. These hydration products have a significant effect on weakening the brittle behavior of SAC, similar to the role of the fibers in the fiber-reinforced cement-based materials. A detailed discussion of the microscopic mechanism on minute quantities of GO improving the mechanical properties of SAC has been given as follows.

3.2 XRD patterns of the GO-SAC samples

Figure 2 shows XRD patterns of SAC and GO-SAC at the ages of 100 min, 6 h, and 24 h. From Figure 2, the main hydration products of SAC are ettringite (AFt) and monosulfide hydrated calcium sulphoaluminate (AFm), and unhydrated C_4A_3S is also presented in the sample. Comparing XRD patterns of SAC at different ages shown in Figure 2, the peak intensity of the raw material C_4A_3S gradually de-

creases with hydration time, and the peaks of hydration products gradually increase. By comparing the XRD patterns of between the GO-SAC sample and the control SAC sample at the same age, it is not difficult to find that the peak enhancement of the hydration products of GO-SAC comes principally from the enhancement of the AFt peak, which is particularly evident at 100 minutes and 6 hours. That is, the incorporation of GO significantly enhances the characteristic peak of the main hydration product AFt compared with the control SAC sample at the ages of 100 minutes and 6 hours.

The formation of AFt is a process in which an aluminum octahedron and a calcium polyhedron are alternately arranged to form a multi-column surface, and then SO_4^{2-} enters into the inter-column trench to balance a positive charge [43, 44]. After the addition of GO, GO as an excellent nucleating agent, the huge surface area provides a large number of nucleation sites, thereby reducing the nucleation free energy of the aluminous octahedron and the critical size of the core, and increasing the nucleation rate. As a result, SAC being hydrated at a faster rate increases its early hydration process. However, After 24 hours of hydration, the characteristic peak of the main hydration product AFt incorporated into GO-SAC cannot be changed significantly compared with SAC, since the SAC slurry is hardened and the initial skeleton is formed after the solidification of 24 hours. It's remarkable that the diffusion rate is also reduced because of the formation of the initial skeleton, thus the formation speed of AFt is gradually close to the formation speed of the blank at the age of 24 hours.

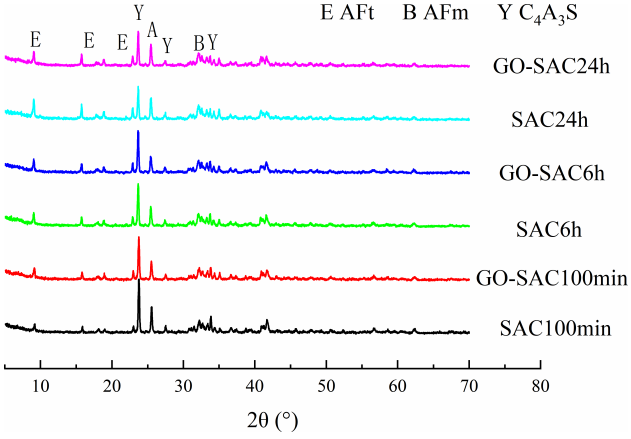

Figure 2: XRD patterns of SAC and GO-SAC at the ages of 100 min, 6 h and 24 h

3.3 SEM observation

Figure 3 shows the SEM images of SAC and GO-SAC at different ages (a-c, microstructure of SAC at 100 minutes, 6

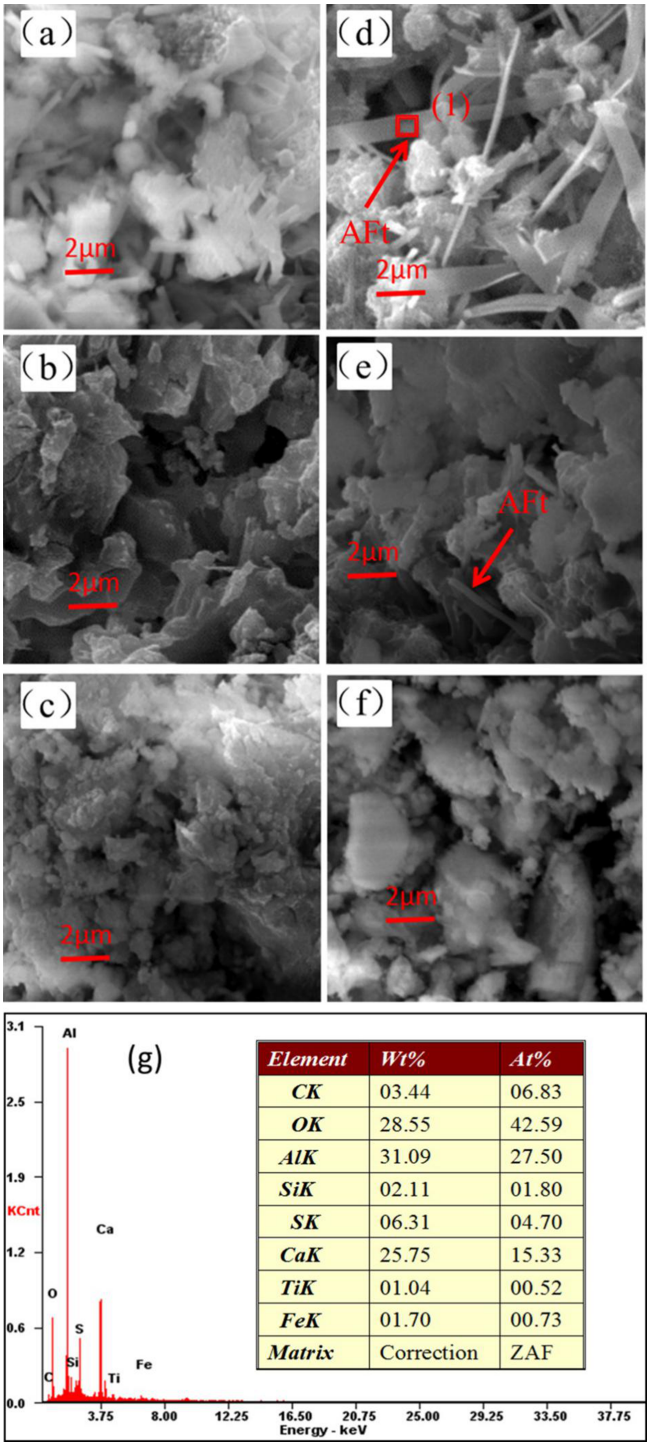

Element	Wt%	At%
CK	03.44	06.83
OK	28.55	42.59
AlK	31.09	27.50
SiK	02.11	01.80
SK	06.31	04.70
CaK	25.75	15.33
TiK	01.04	00.52
FeK	01.70	00.73
Matrix	Correction	ZAF

Figure 3: SEM images of SAC and GO-SAC at different ages. Microstructure of SAC at (a) 100 min; (b) 6 h; (c) 24 h. Microstructure of GO-SAC at (d) 100 min; (e) 6 h; (f) 24 h; (g) EDS analysis of region (1) from (d)

hours, 24 hours; d-f, microstructure of GO-SAC at 100 minutes, 6 hours, 24 hours; g, EDS analysis of (1) from d). It can be suggested that the ribbon-like hydrates are AFt by the elemental composition from Figure 3g [45, 46]. Figure 3a and d show that after 100 minutes, the number of columnar crystals of AFt was increased in control sample, and amount of Aft was generated in GO-SAC, indicating that GO has functioned within 100 minutes of hydration. The ribbon-like AFts have a significant effect on the mechanical properties of SAC at early hydration, resulting in the high enhancement of flexural and compressive strength of specimens at 6 hours. A possible reason is that the GO contains acidic sites through interaction with water, which can take part in cation exchange reactions [47, 48]. That resulted in the hydration environment changes and GO also serves as a template to form new morphology hydrate, such as the ribbon-like AFts [49, 50]. And these AFts can intertwine to form a network structure, leading to mechanical improvement. Figure 3b and e show the microstructure of SAC and GO-SAC that after 6 hours, respectively. The AFts were wrapped up by hydrates, and there was more pore in control sample. Thus, GO shows ability to enhance the AFts' formation at the early hydration of SAC. Figure 3c and f shows that after 24 hours hydration, the two samples have similar morphologies, indicating that the hydration rate of GO-SAC corresponds to that of SAC. Thus, GO does not promote the late hydration of SAC, leads to similar mechanical properties, which is consistent with the previous results of mechanical performance analysis. This also provides viewable evidence to support the XRD analysis that the growth of the compressive strength and flexural strength at the age of 100 minutes and 6 hours is mainly attributed to AFt's formation.

3.4 Pore structure of GO-SAC paste

The pore structure of the selected samples was measured by the BET method in this study. Figure 4 shows the pore size distribution of SAC and GO-SAC at the ages of 6 hours and 24 hours. From pore size distribution curve, one rather similar most probable pore with the size of ~40 nm are observed in the SAC and GO-SAC samples. It can be found from Figure 4a that the 6 hours GO-SAC sample has more the pores with sizes less than 150 nm, compared with the control SAC sample. This means that the previous GO prompted a large amount of AFt to compensate for the coarse holes in the GO-SAC matrix, while the AFts overlap each other to form more micropores. This improves the compressive strength and flexural strength of the GO-SAC sample at the age of 6 hours. However, as shown in Figure 4b, there is no significant difference observed in the pore size distribution and the corresponding pore percentage of SAC and GO-SAC at the age of 24 hours. This corresponds to the little change in the compressive strength and flexural strength at the age of 24 hours. It also indicates that GO only accelerates the early hydration process, accelerating the formation of AFt, and has little effect on the post-hydration.

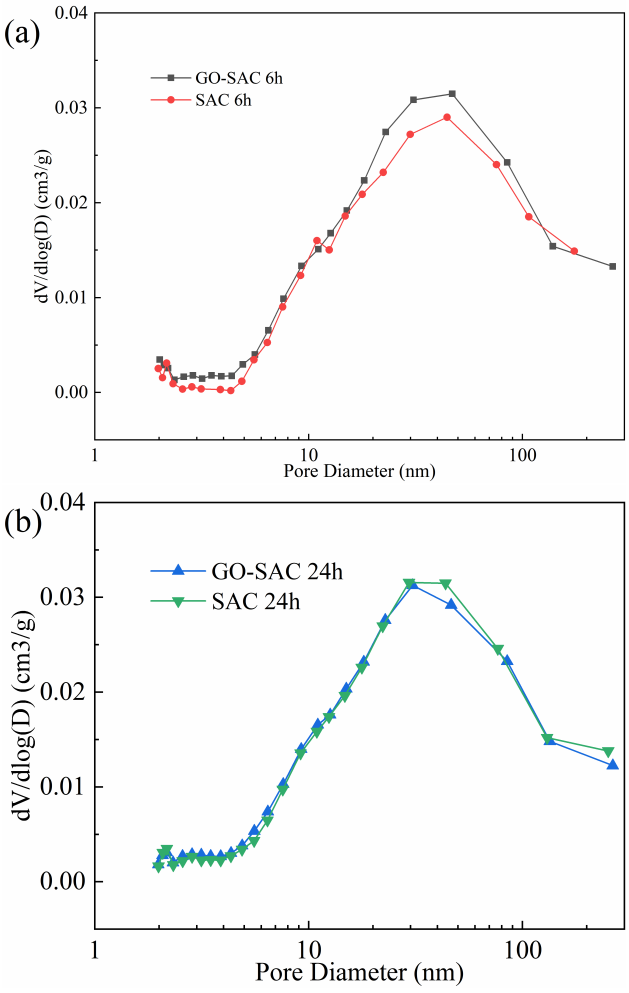

Figure 4: Pore size distribution of SAC and GO-SAC: (a) at 6 h; (b) at 24 h

3.5 DSC-TG analysis of SAC and GO-SAC

Figure 5 shows the DSC, TG and DTG patterns of SAC and GO-SAC at the age of 6 hours. There are three significant endothermic DSC peaks observed from Figure 5. The first peak in the temperature from 50°C to 150°C corresponds to the dehydration reactions of AFt. The loss of crystalline

water of AFt leads to it being transformed to AFm. At about 250°C, the second endothermic peak and the corresponding mass loss are occurred due to the dehydration reaction of the low sulfur type calcium sulphoaluminate [51, 52]. At about 730°C, it is shown that the third endothermic peak and the corresponding mass loss are initiated by the crystal transformation of β-C_2S and the decomposition of calcium carbonate [44].

It is inferred from the first peak shown in Figure 5 that the addition of GO is associated with the significant difference of mass loss at the age of 6 hours. The mass loss of SAC at 6h is about 7% (as shown in Figure 5a), and the mass loss of GO-SAC is about 7.6% (as shown in Figure 5b) in the temperature range of 50°C ~150°C. This difference is caused by the difference of AFt content, indicating that the addition of GO promotes the formation of AFt at the age of 6 hours. As a conclusion, the results of DSC-TG analysis supports the results from XRD and SEM characterizations as well.

3.6 Hydration heat analysis

Figure 6 shows the hydration heat release rate curve of SAC and GO-SAC. According to Figure 6a, there are three consecutive exothermic peaks observed in the control SAC sample. The addition of GO has increased the peak intensity of the first exothermic peak from 6.1 mW/g to 7.0 mW/g, while the second peak is almost unchanged. The third peak is decreased from 8.0 W/g to 7.4 W/g and the appearance of this peak is advanced under the effects of GO. Thus, it seems that GO slightly accelerates the hydration of SAC, making the heat release peak slightly ahead.

Overall, the addition of GO cannot lead to a large change of the hydration heat release rate, which also indicates that GO cannot participate in the hydration reaction during SAC hydration. According to XRD analysis and SEM observation, it can be inferred that GO is mainly involved in the crystallization process of hydration products in the SAC system so that the hydrated product AFt is first crys-

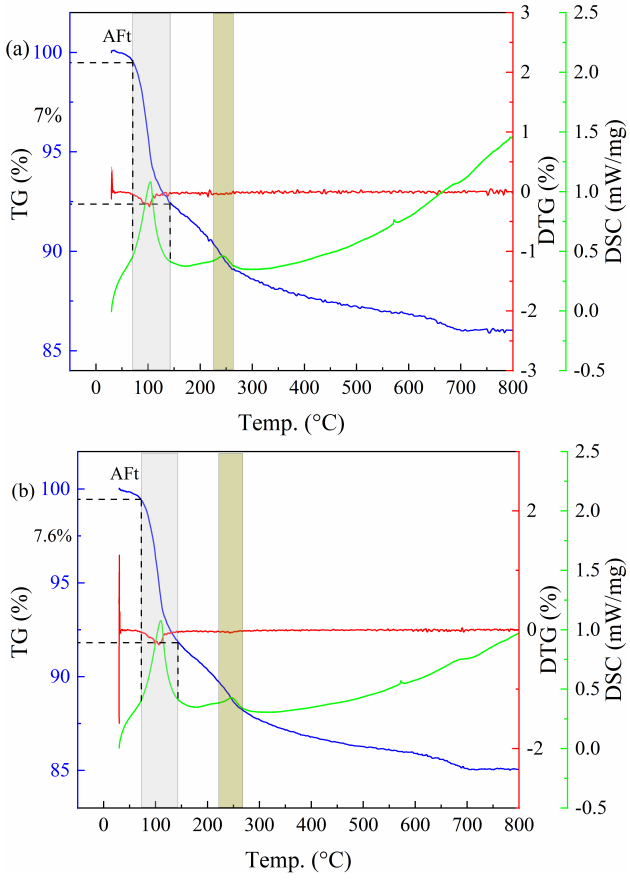

Figure 5: DSC, TG and DTG patterns of samples at the age of 6h. (a) DSC, TG and DTG patterns of SAC; (b) DSC, TG and DTG patterns of GO-SAC

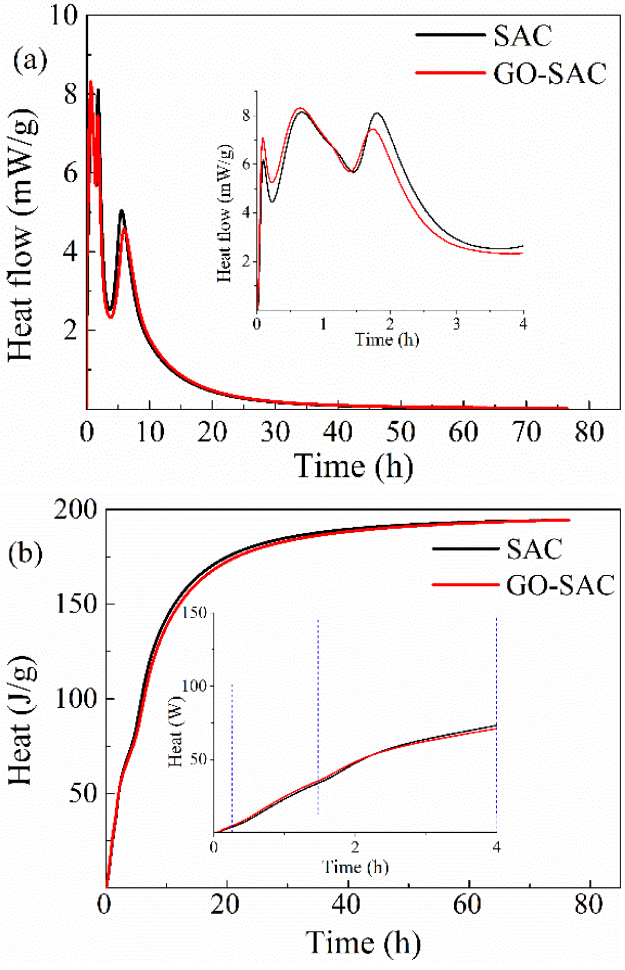

Figure 6: Hydration heat analysis of SAC and GO-SAC: (a) heat flow curves; (b) cumulative heat curves

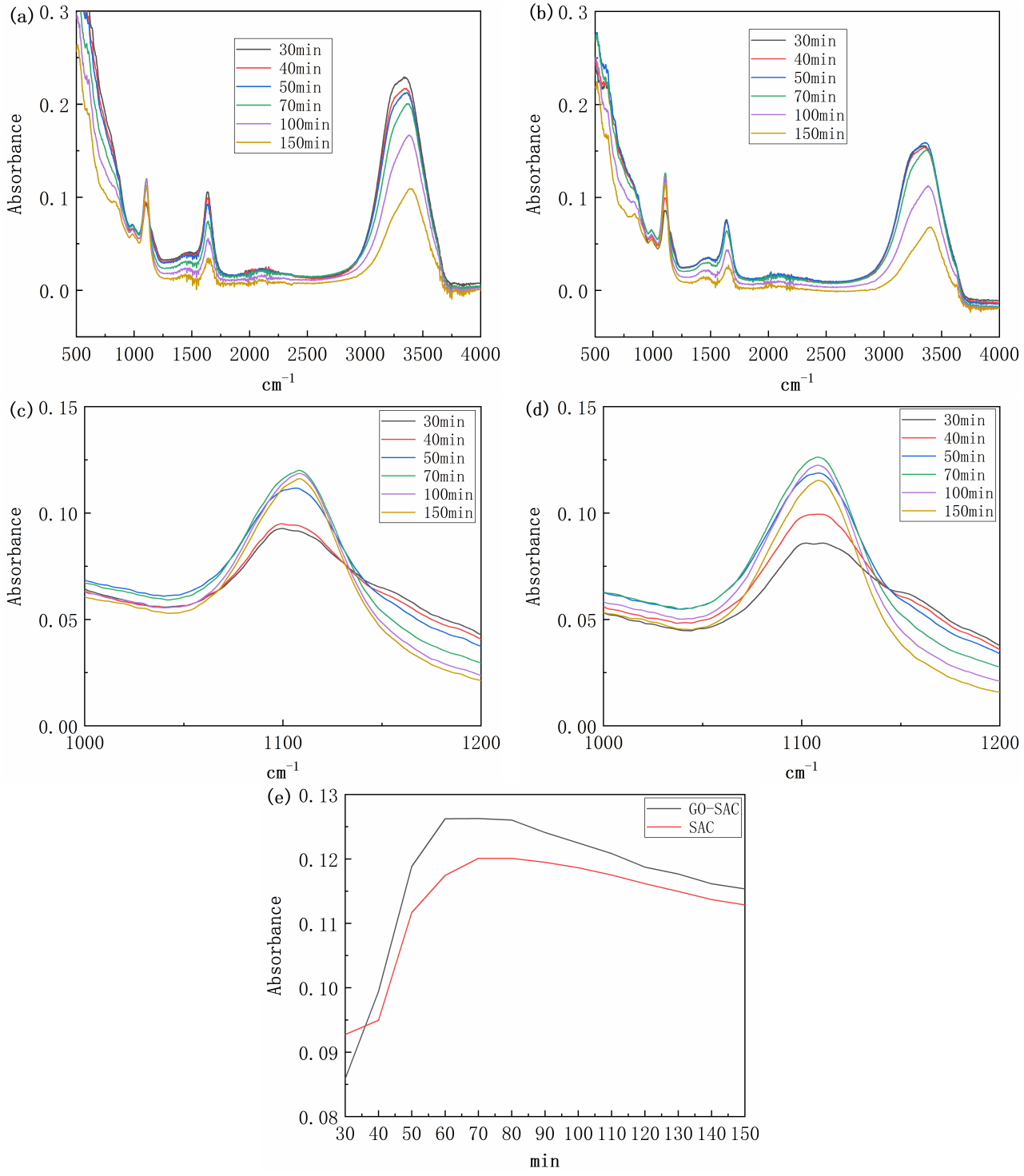

Figure 7: *In situ* ATR investigation. *In situ* ATR spectra of (a) SAC; (b) GO-SAC; the *in situ* ATR spectra from 1000 cm^{-1} to 1200 cm^{-1} of (c) SAC; (d) GO-SAC; (e) the peak-to-time relationships of AFt between SAC and GO-SAC.

tallized. The type of hydration product finally formed by GO-SAC has been not changed, but the crystallization sequence of hydration products has been changed.

3.7 In situ ATR investigation

Figure 7a and b show the change in the ATR spectrum due to the sulfoaluminate cement hydration reaction within 30-150 minutes. The bands at 1650 cm^{-1} and 3000-3600 cm^{-1}

represent free water, while the bands at 1100 cm^{-1} are attributed to AFt of the sulphoaluminate cement hydration product [53–56]. It can be noticed from Figure 7a and b that the peak intensity of AFt gradually reduces and the peak intensities of free water increase as time goes by. This corresponds to the formation of AFt and the consumption of free water during the hydration reaction, respectively.

The data in the 1000-1200 cm^{-1} bands were observed separately to understand the formation and evolution of AFt in SAC (Figure 7c) and GO-SAC (Figure 7d) over time. As shown in Figure 7c and 7d, the peak intensity of AFt in GO-SAC is higher than that in SAC. In order to better compare the promotion of GO on the formation of AFt in GO-SAC, the peak-to-time relationships of AFt between SAC and GO-SAC are extracted from Figure 7c and d and recorded in Figure 7e. It can be noticed from Figure 7e that AFt of GO-SAC reaches its maximum peak at 60 min and that of SAC reaches its maximum peak at 70 minutes, indicating the accelerated formation of AFt with the help of GO. Moreover, the significant differences in the peak intensity of AFt between SAC and GO-SAC can be observed throughout the period of cement hydration within 30-150 minutes. This indicates that more AFt is generated in GO-SAC compared with SAC, giving good support to the results of SEM and XRD at the age of 100 minutes. In addition, in situ ATR results further explain that the reason why the flexural strength is increased by 121% at 100 min is due to a large amount of fibrous AFt formed by the incorporation of GO.

4 Conclusion

In this study, 0.04 wt% GO was incorporated into SAC to improve the ultra-early strength within 24 hours for the use of rapid repair engineering. The tentative conclusions can be summarized as follows.

1. Incorporation of minute quantities of GO can significantly increase the compressive and flexural strength of SAC within 24 hours, the compressive strength of GO-SAC are 25.4%, 46.9% and 5.8% higher than that of SAC at 100min, 6h, and 24h, respectively and the flexural strength of GO-SAC are increased by 121.4%, 13.3% and 1.4% compared with control SAC at 100min, 6h, and 24h.
2. Addition of minute quantities of GO increases the crystallinity of the hydration product AFt of SAC at the early ages such as 100min and 6h, having no effect on the type of hydrated product produced.
3. Fibrous AFt acts as a fiber reinforcement for improved flexural strength and compressive strength before 6 hours. After 24 h, the difference in microstructure between GO-SAC and SAC is reduced, and the enhancement of AFt is weakened.

SAC is used as road repair material, and its cost can be acceptable. Moreover, the addition of the low amount of GO makes the cost of GO-SAC more controllable. GO-SAC exhibits great potential to improve the ultra-early strength of SAC. However, we need to carry on the GO-SAC system more in-depth study, including the effect of the different concentrations of GO on the mechanical properties of SAC at early ages.

Acknowledgement: The financial support from National Key R&D Program of China (No. 2017YFB0309901), the National Natural Science Foundation of China (No. 51872064), the Program of Transportation Department of Liaoning Province (No. 201716) and Natural Science Foundation of Ningbo (No. 2018A610357) for current research is gratefully acknowledged.

Conflict of Interests: The authors declare that there is no conflict of interest regarding the publication of this paper.

References

[1] Cho C.-G., Kim Y.-Y., Feo L., Hui D., Cyclic responses of reinforced concrete composite columns strengthened in the plastic hinge region by HPFRC mortar, Compos. Struct., 2012, 94, 2246-2253.
[2] Xie X., Zhou Z., Jiang M., Xu X., Wang Z., Hui D., Cellulosic fibers from rice straw and bamboo used as reinforcement of cement-based composites for remarkably improving mechanical properties, Compos. Part. B-Eng., 2015, 78, 153-161.
[3] Liu Y., Wang M., Wang W., Ohmic heating curing of electrically conductive carbon nanofiber/cement-based composites to avoid frost damage under severely low temperature, Compos. Part A-Appl. S., 2018, 115, 236-246.
[4] Liu C., Deng X., Liu J., Hui D., Mechanical properties and microstructures of hypergolic and calcined coal gangue based geopolymer recycled concrete, Constr. Build. Mater., 2019, 221, 691-708.
[5] Lang L., Duan H., Chen B., Properties of pervious concrete made from steel slag and magnesium phosphate cement, Constr. Build. Mater., 2019, 209, 95-104.
[6] Juenger M.C.G., Winnefeld F., Provis J.L., Ideker J.H., Advances in alternative cementitious binders, Cement. Concrete. Res., 2011, 41, (12), 1232-1243.
[7] Gartner E., Industrially interesting approaches to “low-CO2” cements, Constr. Build. Mater., 2004, 34, (9), 1489-1498.
[8] Cabrera J.G., Al-Hasan A.S., Performance properties of concrete repair materials, Constr. Build. Mater., 1997, 11, (5), 283-290.
[9] Gastaldini A.L.G., Isaia G.C., Saciloto A.P., Missau F., Hoppe T.F., Influence of curing time on the chloride penetration resistance of concrete containing rice husk ash: A technical and economical

feasibility study, Cement. Concrete. Comp., 2010, 32, (10), 783-793.
[10] Glasser F.P., Zhang L., High-performance cement matrices based on calcium sulfoaluminate–belite compositions, Cement. Concrete. Res., 2001, 31, (12), 1881-1886.
[11] Li G., Zhang J., Song Z., Shi C., Zhang A., Improvement of workability and early strength of calcium sulphoaluminate cement at various temperature by chemical admixtures, Constr. Build. Mater., 2018, 160, 427-439.
[12] Wang K., Lomboy G., Developing Green, Highly Flowable, Rapid Set, High-Performance Concrete for Pavement Patch Repair, InTrans Project Reports., 2016.
[13] Guo T., Xie Y., Weng X., Evaluation of the bond strength of a novel concrete for rapid patch repair of pavements, Constr. Build. Mater., 2018, 186, 790-800.
[14] Making pavements safe: Cement provides fast-setting and durable road repairs, Roads & Bridges, 2018, 56, (10), 56-57.
[15] Kwon B.J., Kim D., Rhee S.K., Kim Y.R., Spray injection patching for pothole repair using 100 percent reclaimed asphalt pavement, Constr. Build. Mater., 2018, 166, 445-451.
[16] Wang S., Liu B., Zhao P., Lu L., Cheng X., Effect of early-strength-enhancing agents on setting time and early mechanical strength of belite–barium calcium sulfoaluminate cement, J. Therm. Anal. Calorim., 2018, 131, (3), 2337-2343.
[17] Aggoun S., Cheikh-Zouaoui M., Chikh N., Duval R., Effect of some admixtures on the setting time and strength evolution of cement pastes at early ages, Constr. Build. Mater., 2008, 22, (2), 106-110.
[18] Dodson V., Concrete Admixture-Set Accelerating Admixtures, VN Reinhold, New York ,1990.
[19] Thilgavathi S., Dhinakaran G., Venkataramana J., Durability of Fly Ash Concrete to Chloride Ingress, Iup. J. Struct. Eng., 2010, 3, (3), 47-65.
[20] Yuan Q., Shi C., De Schutter G., Audenaert K., Deng D., Chloride binding of cement-based materials subjected to external chloride environment-A review, Constr. Build. Mater., 2009, 23, (1), 1-13.
[21] Castellote M., Andrade C., Alonso C., Chloride-binding isotherms in concrete submitted to non-steady-state migration experiments, Cement. Concrete. Res., 1999, 29, (11), 1799-1806.
[22] Xiao L.I., Liang L., Liu Z.D., Niu W.Y., Zhang Q., Zhang Z.B., Effect of Supplementary Curing after Steam-curing on Performance of Concrete, Bulletin Chin. Ceram. Soc., 2015, 852, 1376-1382.
[23] Nazari A., Riahi S., Effects of CuO nanoparticles on compressive strength of self-compacting concrete, Sadhana-Acad. P. Eng. S., 2011, 36, (3), 371.
[24] Naskar S., Chakraborty A.K., Effect of nano materials in geopolymer concrete, Perspectives in Science, 2016, 8, 273-275.
[25] Qin L., Gao X., Chen T., Influence of mineral admixtures on carbonation curing of cement paste, Constr. Build. Mater., 2019, 212, 653-662.
[26] Adamu M., Mohammed B.S., Shafiq N., Shahir Liew M., Effect of crumb rubber and nano silica on the fatigue performance of roller compacted concrete pavement, Cogent Engineering, 2018, 5, (1), 1436027.
[27] Zhang W., Han B., Yu X., Ruan Y., Ou J., Nano boron nitride modified reactive powder concrete, Constr. Build. Mater., 2018, 179, 186-197.
[28] Mokhtar M.M., Abo-El-Enein S.A., Hassaan M.Y., Morsy M.S., Khalil M.H., Mechanical performance, pore structure and microstructural characteristics of graphene oxide nano platelets reinforced cement, Constr. Build. Mater., 2017, 138, 333-339.
[29] Dreyer D.R., Park S., Bielawski C.W., Ruoff R.S., The chemistry of graphene oxide, Chem. Soc. Rev., 2010, 39, (1), 228-240.
[30] Warner J.H., Schaffel F., Rummeli M., Bachmatiuk A., Graphene: fundamentals and emergent applications, 2012, Newnes.
[31] Cruz-Silva R., Endo M., Terrones M., Graphene oxide films, fibers, and membranes, Nanotechnol. Rev., 2016, 5, 377-391.
[32] Zepeng J., Bin Z., Chunya L., Weicong K., Jingxian Z., Yongqiang X., Shaozao T., Xiang C., Langhuan H., Carboxymethyl cellulose-grafted graphene oxide for efficient antitumor drug delivery, Nanotechnol. Rev., 2018, 7, 291-301.
[33] Suk J.W., Piner R.D., An J., Ruoff R.S., Mechanical properties of monolayer graphene oxide, Acs. Nano., 2010, 4, (11), 6557-6564.
[34] Chen W., Lv G., Hu W., Li D., Chen S., Dai Z., Synthesis and applications of graphene quantum dots: a review, Nanotechnol. Rev., 2018, 7, 157-185.
[35] Ghazizadeh S., Duffour P., Skipper N., Billing M., Bai Y.J.C., Research C., An investigation into the colloidal stability of graphene oxide nano-layers in alite paste, Cement. Concrete. Comp., 2017, 99, 116-128.
[36] Shaikh F.U., Supit S.W., Barbhuiya S., Microstructure and nanoscaled characterization of HVFA cement paste containing nano-SiO2 and nano-CaCO3, J. Mater. Civil. Eng., 2017, 29, (8), 04017063.
[37] Lv S., Ma Y., Qiu C., Sun T., Liu J., Zhou Q., Effect of graphene oxide nanosheets of microstructure and mechanical properties of cement composites, Constr. Build. Mater., 2013, 49, 121-127.
[38] Lv S., Liu J., Sun T., Ma Y., Zhou Q., Effect of GO nanosheets on shapes of cement hydration crystals and their formation process, Constr. Build. Mater., 2014, 64, 231-239.
[39] Sharma S., Kothiyal N.C., Comparative effects of pristine and ball-milled graphene oxide on physico-chemical characteristics of cement mortar nanocomposites, Constr. Build. Mater., 2016, 115, 256-268.
[40] Lv S., Hu H., Hou Y., Lei Y., Sun L., Zhang J., Liu L.J.N., Investigation of the Effects of Polymer Dispersants on Dispersion of GO Nanosheets in Cement Composites and Relative Microstructures/Performances, Nanomaterials, 2018, 8, 964.
[41] Gong K., Pan Z., Koraye, A.H., Qiu L., Li D., Collins F., Wang C.M., Duan W.H., Reinforcing effects of graphene oxide on portland cement paste, J. Mater. Civil. Eng., 2014, 27, (2), A4014010.
[42] Pan Z., He L., Qiu L., Korayem A.H., Li G., Zhu J.W., Collins F., Li D., Duan W. H., Wang M.C., Mechanical properties and microstructure of a graphene oxide–cement composite, Cement Concrete Comp., 2015, 58, 140-147.
[43] Coumes C.C.D., Dhoury M., Champenois J.-B., Mercier C., Damidot D., Combined effects of lithium and borate ions on the hydration of calcium sulfoaluminate cement, Cement. Concrete. Res., 2017, 97, 50-60.
[44] Li G., He T., Hu D., Shi C., Effects of two retarders on the fluidity of pastes plasticized with aminosulfonic acid-based superplasticizers, Constr. Build. Mater., 2012, 26, (1), 72-78.
[45] Jiahui P., Zonghan L., Study on the Formation Mechanism of Ettringite, J. Chin. Ceram. Soc. (in Chinese), 2000, 28, (6), 511-515.
[46] Popoola O.O., Kriven W.M., Young J.F., Microstructural and Microchemical Characterization of a Calcium Aluminate-Polymer Composite (MDF Cement), J. Am. Ceram. Soc., 1991, 74, (8), 1928-1933.
[47] Han J., Yan P., Influence of lithium compound on sulphoaluminate cement hydration process, Journal of the Chinese Ceramic Society, 2010, 38, (4), 608-614.

[48] Ghazizadeh S., Duffour P., Skipper N.T., Bai Y., Understanding the behaviour of graphene oxide in Portland cement paste, Cement. Concrete. Res., 2018, 111, 169-182.
[49] Ma B., Zhu Y., Hu D., Li H., Influence of calcium formate on sulphoaluminate cement hydration and harden process at early age, J. Appl. Biomater. Fun., 2013, 44, 1763-1767.
[50] Lv S., Ting S., Liu J., Zhou Q., Use of graphene oxide nanosheets to regulate the microstructure of hardened cement paste to increase its strength and toughness, Crystengcomm., 2014, 16, (36), 8508-8516.
[51] Shen C., Pan M., Hua Z., Yuan R., Aluminate cement/graphite conductive composite bipolar plate for proton exchange membrane fuel cells, J. Power. Sources., 2007, 166, (2), 419-423.
[52] Wang P., Li N., Xu L., Hydration evolution and compressive strength of calcium sulphoaluminate cement constantly cured over the temperature range of 0 to 80°C, Cement. Concrete. Res., 2017, 100, 203-213.
[53] Ylmén R., Jäglid U., Panas I., Monitoring Early Hydration of Cement by Ex Situ and In Situ ATR-FTIR – a Comparative Study, J. Am. Ceram. Soc., 2014, 97, (11), 3669-3675.
[54] Björnström J., Panas I., Antagonistic effect of superplasticizer and colloidal nano-silica in the hydration of Alite and Belite pastes, J. Mater. Sci., 2007, 42, (11), 3901-3907.
[55] Oltulu M., Şahin R., Effect of nano-SiO2, nano-Al2O3 and nano-Fe2O3 powders on compressive strengths and capillary water absorption of cement mortar containing fly ash: A comparative study, Energ. Buildings, 2013, 58, 292-301.
[56] Senff L., Hotza D., Lucas S., Ferreira V., Labrincha J. A., Effect of nano-SiO2 and nano-TiO2 addition on the rheological behavior and the hardened properties of cement mortars, Mat. Sci. Eng. A, 2012, 532, 354-361.